Effect of SiO_2 on the Electrical and Magnetic properties of Nanocrystalline $NiFe_2O_4$

I. Prakash[1], M. Venkateswarlu[2] and N. Satyanarayana[1*]

[1]Department of Physics, Pondicherry University, Puducherry 605014, India
[2]R& D, Amara Raja Batteries Ltd, Tirupati 517520 A.P, India

ABSTRACT

$SiO_2/NiFe_2O_4$ nanocomposite is prepared using base catalyst assisted in-situ sol-gel process with the help of sonication. The prepared sample is characterized using XRD, FTIR and HRTEM analysis. The electrical and magnetic properties are measured using impedance analysis and vibrating sample magnetometer (VSM) for the $SiO_2/NiFe_2O_4$ nanocomposite and it is compared with the results of nanocrystalline $NiFe_2O_4$ prpeared using citric acid urea assisted combustion process. The variation of electrical and magnetic properties of nanocrystalline $NiFe_2O_4$ and $SiO_2/NiFe_2O_4$ nanocomposite are explained based on the microstructure of the material. Also, the electrical properties are explained for the nanocrystalline $NiFe_2O_4$ and $SiO_2/NiFe_2O_4$ nanocomposite and compared with the reported results of $NiFe_2O_4$ and SiO_2 anodes used in the lithium ion battery applications.

Keywords: $NiFe_2O_4$ nanocrystal $SiO_2/NiFe_2O_4$ nanocomposite, Sol-gel process, XRD, FTIR, HRTEM VSM, Impedance.

1 INTRODUCTION

Lithium ion batteries are inevitably used as an energy storage material to fulfill the current energy demands. Active research is going on in making new electrode and electrolyte materials to improve the performance of the battery with moderate capacity and better cycle life [1]. Pure SiO_2, carbon coated SiO_2, silicon alloys and silicon metal with other carbon, graphite additives and core shell, porous structures of silicon based composite compounds are used as anode material in lithium ion battery because of high theoretical capacity of silicon (4200 mAh/g). The problem in the silicon based anode material is its enormous volume change ~ 300% of its original volume results in poor cycle stability. The bare ferrites and ferrites with carbon and SnO_2 additives, also Sn^{4+} doped ferrites are also used as anode materials in lithium ion battery because of their good reversible capacity [2-8]. In both the anodes, the reaction mechanisms involved in the first cycle is the electrochemical reduction of metal oxides into constituent metals and during further cycles, the charging and discharging reaction depends on the formation and decmposition of Li_2O and Li_xSi alloying and dealloying. The proposed reaction mechanism during charge and discahrge cycles of both SiO_2 and ferrite based anode materials and confirmed from cyclic voltametry measurements are given below[3,7].

$SiO_2 + 4Li^+ + 4e^- \rightarrow 2Li_2O + Si$ ----------1

$2SiO_2 + 4Li^+ + 4e^- \rightarrow Li_4SiO_4 + Si$ ----------2

$Si + xLi^+ + xe^- \leftrightarrow Li_xSi$ ----------3

$NiFe_2O_4 + 8Li^+ \rightarrow Ni + 2Fe + 4Li_2O$ ----------1

$Ni + 2Fe + 4Li_2O \leftrightarrow NiO + Fe_2O_3 + 8Li^+$ -----2

In the case of alloy formation, continuous alloying results in the pulverization of the anode material causes the poor contacts with the current collecor, which diminishes the capacity within first few cycles. Hence, porous structured composite material consists of two different phases with different additives are developed to enhance the conductivity as well as to accomodate the volume changes when it is used as a anode in lithium ion battery. In our present paper, the ferrites coated and dispersed in amorphous SiO_2 composite material is prepared using base catalyst assisted sol-gel process under sonication. Electrical and magnetic properties of $SiO_2/NiFe_2O_4$ nanocomposites are compared with the reported results of nancrystalline $NiFe_2O_4$ [9].

2. EXPERIMENTAL SYNTHESIS

2.1. Base catalyst assisted sol-gel process

10% $NiFe_2O_4$ – 90% SiO_2 nanocomposite sample is prepared using base catalyst assisted sol-gel process. All the used precursor chemicals are AR grade nickel nitrate hexahydrate, ferric nitrate nanohydrate, tetraethoxyorthosilane (TEOS) and ethanol. 20 ml TEOS is mixed with 20 ml of ethanol (Equal volume ratio is maintained) and sonicated for a minute. Later, 1 ml of NH_4OH (25%) solution is slowly added to the TEOS and ethanol solution and sonicated for a minute to initiate the seed formation for SiO_2 particle growth. The remaining 9 ml of NH_4OH is added to the above solution and sonicated for two more minutes to form the SiO_2 slurry. The required quantity of nickel nitrate hexahydrate and ferric nitrate nanohydrate are separately dissolved in ethylene glycol and sonicated for 10 minutes each. Nickel and ferric nitrate solutions are mixed and the mixed solution is again sonicated for 10 more minutes. The nickel and ferric nitrate solution mixture is slowly added to the SiO_2 slurry under constant stirring and further, the slurry mixture is sonicated for 30 minutes. Finally, the slurry mixture is stirred at

* Corresponding author (Prof. N. Satyanarayana) E-mail: nallanis2011@gmail.com Phone: +91-413-2654404

353 K to get the dry powder. The resulted powder is dried and calcined at 473, 673 and 873 K for 3 hr. to obtain $SiO_2/NiFe_2O_4$ composite.

2.2. Characterization

The powder X-ray diffraction patterns are recorded for the $SiO_2/NiFe_2O_4$ gel sample calcined at different temperatures using PANalytical XpertPro X-ray diffractometer with Cu K_α radiation of wavelength λ=1.5418 A^o and scanned from 80-10^0 at a scan rate of 1.5 degree per minute. For FTIR measurements, thin transparent pellets are prepared using dried gel sample, heated from room temperature to 873 K, grinded well with spectra pure KBr powder taken in 1:20 ratio. FTIR spectra are recorded for the sample pellets using Shimadzu spectrophotometer in the range of 4000 – 400 cm^{-1} for 20 scans. The HRTEM images are taken for the $SiO_2/NiFe_2O_4$ sample dispersed in acetone sprayed over a copper grid. Selected area electron diffraction (SAED) pattern is taken using transmission electron microscope of JEOL 2010F HRTEM, Japan, with 200 KV as operating voltage.

3. RESULT AND DISCUSSION

3.1. XRD

Figure 1 shows the powder X-ray diffraction patterns of the $SiO_2/NiFe_2O_4$ gel sample calcined at different temperatures.

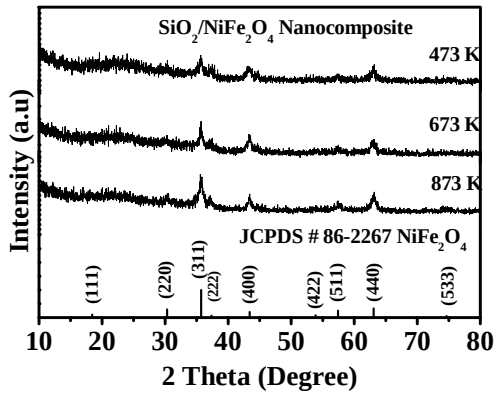

Fig. 1. Powder X ray diffraction patterns of $SiO_2/NiFe_2O_4$ nanocomposite obtained at different temperatures.

The XRD patterns of the sample calcined at 473 K, 673 K and 873 K showed the characteristic crystalline diffraction pattern of $NiFe_2O_4$ and amorphous SiO_2. The broad reflection peak observed at 22 ^{o} is corresponds to the characteristic diffraction pattern of amorphous SiO_2 [9]. The amorphous pattern of SiO_2 is not disturbed during calcination. The formation of crystalline $NiFe_2O_4$ phase is confirmed by comparing the observed diffraction pattern with the standard JCPDS # 86-2267 data of $NiFe_2O_4$. The crystallite size is calculated using Scherrer's formula and it is found to be ~ 14 nm for the $SiO_2/NiFe_2O_4$ sample obtained at 873 K, which confirms the formation of nanocrystalline $NiFe_2O_4$ phase. The $NiFe_2O_4$ nanocrystal growth is observed with increase of temperature without disturbing the amorphous SiO_2 phase and confirms the formation of $SiO_2/NiFe_2O_4$ nanocomposite.

3.2. FTIR

Figure 2 shows the FTIR spectra of the $SiO_2/NiFe_2O_4$ gel sample heated at different temperatures. The gel sample calcined at 473 K showed the vibration bands at 3390, 3176, 2895, 1636, 1385, 1180, 1081, 957, 883 and 450 cm^{-1}. The band at 3390 cm^{-1} corresponds to the stretching vibration of O-H molecules and it is associated with the presence of water in the sample. The band at 3176 cm^{-1} is corresponds to NH_3 vibrations from the ammonia group. The band at 2895 corresponds to the stretching vibration of aliphatic CH groups from ethylene glycol present in the $SiO_2/NiFe_2O_4$ gel sample. The IR band at 1636 cm^{-1} is due to the Si-OH vibrations. The band at 1385 cm^{-1} is associated with anti symmetric NO_3^- stretching vibration directly arising from the residual nitrate groups. The absorption band at 1081 cm^{-1} is assigned for ≡Si-O-Si≡ of the SiO_4 tetrahedron and a shoulder band at 1180 cm^{-1} corresponds to the asymmetric stretching bonds of Si-O-Si. The shoulder at 957 cm^{-1} corresponds to Si-O-Fe and Si-O-H stretching. The observed band at 883 cm^{-1} is corresponds to the C-C vibration.

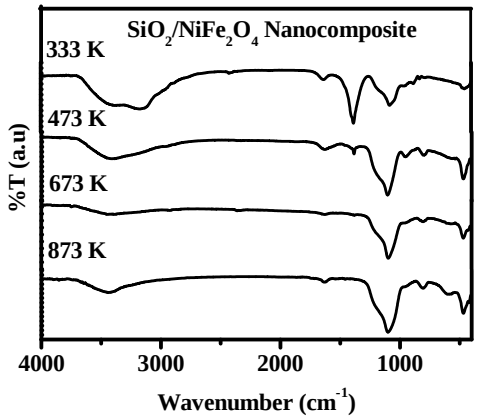

Fig. 2. FTIR spectra of $SiO_2/NiFe_2O_4$ nanocomposite obtained at different temperatures.

The absorption band at 450 cm^{-1} corresponds to Si-O-Si and O-Si-O bending mode [9-12]. The $SiO_2/NiFe_2O_4$ sample heated at 873 showed the bands at 605 and 420 cm^{-1} and the bands correspond to water molecules are diminished because of evaporation. The band at 1080 cm^{-1} is gets intensified for the $SiO_2/NiFe_2O_4$ sample during calcination, which confirms better polymerization of Si-O-Si network in the $SiO_2/NiFe_2O_4$ sample after the removal of OH and C_2H_5OH group from the sample. The absence of organic vibrations observed in the $SiO_2/NiFe_2O_4$ sample calcined at 873 K confirmed its removal from the gel sample during calcination. The observed two peaks at 605 cm^{-1} and 420 cm^{-1} were attributed to the vibrational modes of metals in tetrahedral and octahedral sites of ferrites, which indicate the formation of $NiFe_2O_4$ structure [13]. Hence, FTIR

results confirm the formation of SiO_2 network and $NiFe_2O_4$ structure and hence, confirm the formation of the nanocomposite $SiO_2/NiFe_2O_4$ structure.

3.3. HRTEM

Fig. 3a shows the TEM images of nanocrystalline $NiFe_2O_4$ sample calcined at 623 K and fig 3b and 3c show the HRTEM images taken at two different magnifications for $SiO_2/NiFe_2O_4$ sample obtained at 873 K. Fig. 3a shows the formatin of naocrystals grown at different orientations and separated by a grain boundary. From fig. 3 b and c, HRTEM image taken at lower magnification clearly show the formation of $NiFe_2O_4$ tiny black particles deposited on the agglomerated SiO_2 particles. The high magnified HRTEM images taken at the surface of the $SiO_2/NiFe_2O_4$ nanocomposite sample shows the black tiny particles and surrounded with amorphous silica which are marked in the HRTEM images. This is due to the unreacted TEOS group coated over the already coated $NiFe_2O_4$ precursors during in-situ sonication. Further calcination results in the formation of $NiFe_2O_4$ particles deposition on the SiO_2 and SiO_2 coating over the already coated $NiFe_2O_4$ particles.

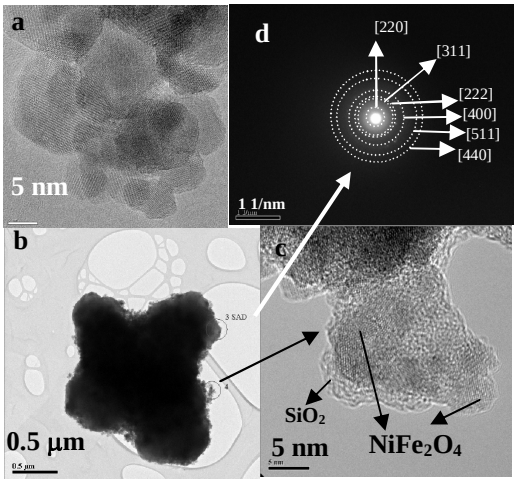

Fig. 3a TEM images of nanocrystalline $NiFe_2O_4$ obtained at 623 K. Fig. 3b & 3c HRTEM images taken at to different magnification for $SiO_2/NiFe_2O_4$ sample obtained at 873 K. Fig. 3d Selected Area Diffraction Pattern for $SiO_2/NiFe_2O_4$ sample obtained at 873 K.

Fig. 3d shows the selected area electron diffraction (SAED) pattern of the $SiO_2/NiFe_2O_4$ sample. From fig. 3d, the SAED patterns are well matched with the standard $NiFe_2O_4$, which confirms that the tiny black particles deposited on the SiO_2 spheres are $NiFe_2O_4$ nanocrystals. Further, the HRTEM images clearly revealed the formation of amorphous SiO_2 particles of size 300-500 nm and also the deposited $NiFe_2O_4$ particles of size ~15-20 nm. Hence, HRTEM and SAED results confirmed the formation of $NiFe_2O_4$ nanocrystals in the $SiO_2/NiFe_2O_4$ nanocomposite sample.

3.4 Electrical and Magnetic Properties

The impedance spectra of $SiO_2/NiFe_2O_4$ nanocomposite and nanocrystalline $NiFe_2O_4$ are shown in fig. 4a and 4b respectively. The impedance spectrum of $NiFe_2O_4$ nanocrystalline ferrite showed two semicircles corresponds to the series combination of two RC parallel circuits. The semicircle observed at low frequency region is corresponds to the grain boundary contribution and the semicircle observed at high frequency region corresponds to the grain interior contribution.

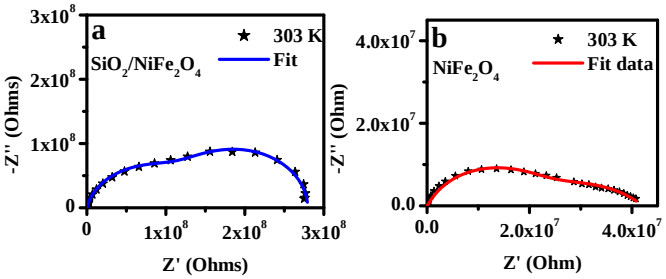

Fig. 4 a and b Impedance spectra of $SiO_2/NiFe_2O_4$ nanocomposite sample obtained at 873 K and nanocrystalline $NiFe_2O_4$ obtained at 623 K and measured at ambient temperature.

Sample	$NiFe_2O_4$	$SiO_2/NiFe_2O_4$
Bulk Resistance (Ohm)	2.042 E+07	1.33 E+08
GB Resistance (ohm)	2.163 E+07	1.50 E+08
Bulk Conductivity (Scm^{-1})	2.00 E-08	4.26 E-09
GB Conductivity (Scm^{-1})	1.89 E-08	3.77 E-09

Table 1: List of Bulk, grain boundary resistance and conductivity values

The grain boundary and grain interior resistances are measured from the intersection of Z'' on the x axis. The observed grain interior (bulk) resistance is smaller than the grain boundary resistance. The nanocrystalline $NiFe_2O_4$ consists of smaller grains that are confirmed from the TEM images. The nanocrystalline material is having more surface area and the surface to volume ratio is more. Hence, more number of atoms are located on the surface, which increases the grain boundary resistance little bit compared to the grain interior resistance. The values of grain interior and grain boundary resistances as well as conductivity values are tabulated in Table 1. The impedance sectrum of $SiO_2/NiFe_2O_4$ nanocomposite showed two semicircles corresponds to the series combination of two RC parallel circuits. The semicircle observed at low frequency region corresponds to the grain boundary contribution and the semicircle observed at high frequency corresponds to the grain interior contribution. The intersection of the Z'' on the x axis gives the grain boundary resistance and grain

interior resistance. Here the grain boundary resistance is more compared to the grain interior resistance. This is because the $SiO_2/NiFe_2O_4$ nanocomposite sample showed the dispersion of $NiFe_2O_4$ nanocrystals on the amorphous SiO_2 as well as inside the SiO_2 matrix. Here, SiO_2 is electrically insulating and dissimilar material contacts at the boundaries results in the increment of grain boundary reistance compared to the grain interior resistance. In the case of transition metal oxides based lithium ion battery anode, the first cycle involves the electrochemical reduction of metal oxides to metals rather than usual lithium ion insertion and deinsertion. On further charge and discharge reaction involves the formation of Li_2O and decomposition of Li_2O for ferrite based anodes and alloying and dealloying reaction for silicon based anodes. Initial contact for electron transfer between the anode material and the current collector is achived by mixing the anode material with current conducting additives. Hence, for electrically insulating anode materilas like SiO_2 the initial electronic contact is achieved by carbon additives. On further cycles, the insulating transition metal oxides transform into conducting metals and further cycles, it is transformed into conducting metal alloys. In our present work, both SiO_2 and ferrites are proposed for anode materials. Hence, alloy formation as well as Li_2O formation occur in the same material. So, the volume change due to continuous alloying can be minimized and it can increase the cycle life. Fig. 5 a and b shows the VSM curves of the $SiO_2/NiFe_2O_4$ nanocomposite obtained at 873 K and nanocrystalline $NiFe_2O_4$ obtained at 623 K and measured at ambient temperature. The saturation magnetization and retinivity and coersive force of $SiO_2/NiFe_2O_4$ nanocomposite is lesser than the values of nanocrystalline $NiFe_2O_4$.

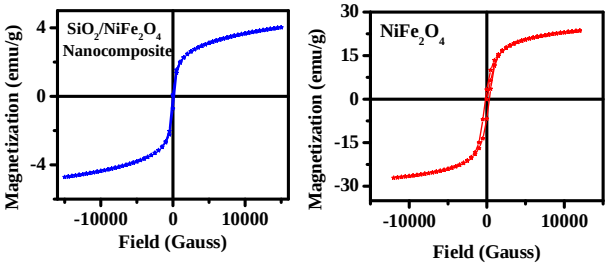

Fig. 5 a and b VSM curves of $SiO_2/NiFe_2O_4$ nanocomposite sample obtained at 873 K and nanocrystalline $NiFe_2O_4$ obtained at 623 K and measured at ambient temperature.

Sample	$NiFe_2O_4$	$SiO_2/NiFe_2O_4$
Saturation Magnetization (emu/g)	25.336	4.3714
Retinivity (emu/g)	5.0132	0.40
Coersivity (Gauss)	244.33	97.43

Table 2: Magnetic values of nanocrystalline $NiFe_2O_4$ and $SiO_2/NiFe_2O_4$ nanocomposite

In the $SiO_2/NiFe_2O_4$ nanocomposite the presence of nonmagnetic SiO_2 reduces the total magnetic material and it decreases the saturation magnetization. The crystallite size of $NiFe_2O_4$ in the $SiO_2/NiFe_2O_4$ nanocomposite is smaller than the crystallite size of nanocrystalline $NiFe_2O_4$, which decreases the retinivity and cersive force. The measured magnetic values are tabulaed in table 2.

CONCLUSION

$SiO_2/NiFe_2O_4$ nanocomposite sample is prepared successfully using base catalyst assisted in-situ sol-gel process and the composite phase formation is confirmed from XRD, and FTIR analysis. The HRTEM images clearly show the crystal growth formation on SiO_2 as well as inside SiO_2. The electrical and magnetic properties of $SiO_2/NiFe_2O_4$ nanocomposite are compared with the nanocrystalline $NiFe_2O_4$ and the changes are attributed to the crystallite size and grain boundaries.

Acknowlegment

NS is gratefully acknowledge DST, UGC, AICTE, CSIR, and DRDO, Govt. of India, for receiving the financial support in the form of major research projects. IP acknowledge CSIR, Govt. of India, for receiving the Research Associate (RA) fellowship. Authors also acknowledge CIF – Pondicherry University for utilizing the VSM facility.

REFERENCES

[1] J. M. Tarascon, M. Armand, Nature, 414, 359, 2001.
[2] H C Tao, L-Z Fan, X Qu, Electrochimica Acta 71, 194, 2012.
[3] B Guo, J Shu, Z Wang, H Yang, L Shi, Y Liu, L Chen, Eelectrochemistry Communications 10, 1876, 2008.
[4] X-Y Zhou, J- J Tang, J Yang, J Xie, L-L Ma, Electrochimica Acta 87, 663, 2013.
[5] H-C Tao, M Huang, L-Z Fan, X Qu, Solid State Ionics 220, 1, 2012.
[6] X.D. Li, W.S. Yang, F. Li, D.G. Evans, X. Duan, Journal of Physics and Chemistry of Solids 67, 1286, 2006.
[7] H Zhao, Z Zheng, K W Wong, S Wang, B Huang, D Li, Electrochemistry Communications 9, 2606, 2007.
[8] R. Kalai Selvan, C.O. Augustin, C. Sanjeeviraja, D. Prabhakaran, Solid State Communications 137, 512, 2006.
[9] I.Prakash, N.Nallamuthu, P.Muralidharan, M. Venkateswarlu, N.Satyanarayana, Nanotech 2009, 1,129, 2009.
[10] I. Prakash, N. Nallamuthu, P. Muralidharan, M. Venkateswarlu, M. Mishra, A. K. Mohanty, N. Satyanarayana, J Sol-Gel Sci Technol 58, 24, 2011.
[11] I. Prakash, N. Nallamuthu, P. Muralidharan, M. Venkateswarlu, N. Satyanarayana, AIP Conference proceedings, 1276, 1, 227, 2010.
[12] I. Prakash, N. Nallamuthu, P. Muralidharan, M. Venkateswarlu, N. Satyanarayana, Nanotech 2011, 1, 542, 2011.
[13] R.D.Waldron, Phys. Rev. 9, 1727, 1955.